Polymer 49 (2008) 5344–5352

Contents lists available at ScienceDirect

Polymer

journal homepage: www.elsevier.com/locate/polymer

Influence of biaxial stretching mode on the crystalline texture in polylactic acid films

X. Ou, M. Cakmak*

Polymer Engineering Department, University of Akron, Akron, OH 44325, United States

ARTICLE INFO

Article history:
Received 15 August 2008
Received in revised form 16 September 2008
Accepted 21 September 2008
Available online 8 October 2008

Keywords:
Biaxial stretching
Polylactic acid
X-ray analysis

ABSTRACT

Structural evolution during simultaneous (SB) and sequential rubbery state biaxial stretching (SEQ) of polylactic acid (PLA) films from cast amorphous precursors was investigated. Simultaneous biaxial stretching always leads to films with in-plane isotropy and poor crystalline order. In the first stage of sequential biaxial stretching, oriented crystallization gradually develops while transverse isotropy is maintained. Application of transverse stretching to these films possessing semicrystalline structure gradually destroys the crystalline structure oriented in MD during this realignment while establishing a second population of oriented but poorly ordered crystallites in TD. This destruction is caused primarily by splaying action under transverse stretching as evidenced by the decrease of crystallite sizes in MD.

1. Introduction

Significant attention has recently been paid to all technical and commercialization aspects of PLA due to its biodegradability and biocompatibility as well as the fact that it can be derived from several renewable resources including corn. It possesses good mechanical barrier properties and excellent transparency [1–3]. Its high price in the past limited its main utility in the medical field. Relatively recent advances in lactic acid purification are expected to bring its price in line with the petroleum based counterparts to be competitive [4]. And this -in turn- is expected to open up wider applications for this material with a potential to replace conventional petroleum derived polymers in such applications as packaging film.

PLA has a glass transition temperature (T_g) of 50–60 °C. Depending on its D content and molecular weight, its cold crystallization temperature (T_c) ranges between 95 and 105 °C, while its melting temperature (T_m) ranges from 150 to 190 °C [1–3]. ΔH_f of PLA is reported to be 93 J/g [5]. PLA chains have higher refractive index along chain axis. This leads to positive intrinsic birefringence of 0.03 for amorphous PLA. Crystallizability of PLA is determined by its chain regularity and mobility. As lactic acid is chiral, regularity of PLA chains is significantly affected by the ratio of L component over D component [6], leading to suppression of crystallizability when small fraction of D is present in most L chains. PLA is a slow crystallizing polymer like PET. It can be quenched into quasi-amorphous state, or crystallized upon annealing and/or orientation. When crystallized quiescently from unnucleated state, PLA generally becomes opaque as a result of light scattering due to the formation of large spherulites. Oriented crystallization significantly increases the nucleation density, leading to transparent products [1–3].

PLA was found to exhibit four crystalline structures, α, β, γ and stereo-complex. The orthorhombic α crystal structure is the most commonly observed structure, in which the chains are in −10/3 left helical conformation. Cell dimension of α crystals has been published by several groups. The values provided vary a little from group to group, as: $a = 10.34$–10.7 Å, $b = 5.97$–6.45 Å, $c = 27.8$–28.8 Å [6–9]. Under high stress, β crystal orthorhombic ($a = 10.31$ Å, $b = 6.1$ Å, $c = 9$ Å) structure with chains exhibiting more extended 3/1 helical conformation can be formed. β crystals are found to transform into α crystal when annealed above T_g [6]. The triclinic stereo-complex can only be obtained with 1:1 mixture of PLLA and PDLA [7]. The hexagonal γ crystals are grown on a special substrate [10].

Ideally, slow crystallizing polymers are quenched into glassy state and subsequently heated to temperatures between T_g and T_{cc} (cold crystallization temperature) where they exhibit rubbery behavior and substantial stress can be applied to the polymers as a result of prevalent high viscosities [11–18].

In this rubbery temperature range, this class of polymers that also includes PET, PEN, PEEK, undergo stress induced crystallization

* Corresponding author.
E-mail address: cakmak1@uakron.edu (M. Cakmak).

0032-3861/$ – see front matter © 2008 Elsevier Ltd. All rights reserved.
doi:10.1016/j.polymer.2008.09.053

beyond a critical chain orientation and thus reduction in entropy. This phenomenon usually accompanies strain hardening at high deformation levels, causing self-leveling which induces uniform thickness [11–16,19–32]. This phenomenon was first attributed by Flory[30–32] to decreased entropy effect upon uncoiling and orientation of polymer chains. Up to now, there is no satisfactory model from first principles for describing SIC behavior in slow crystallizing polymers particularly when they are stretched in rubbery state close to T_g where orientation relaxation rates are very low [20–22,33].

In industrial film processing, both sequential and simultaneous biaxial stretching modes are widely used. SB stretching occurs in single bubble and double bubble film blowing [34–37]. In single bubble film blowing, material is first extruded through an annular die and then the molten polymer was extended over a mandrel of air trapped inside the blown film bubble. In order to produce thin film with slow crystallizing polymers like PLA that possess very low melt strength and crystallization rate, the double bubble film blowing was developed. In this process, the material is quenched into amorphous state in the first bubble, then, it is heated into rubbery state and extended in the second bubble. Sequential biaxial stretching occurs in tenter frame process. In this process, the polymer is first extruded from a sheet die, then cooled and oriented in the machine direction by the relative motion of the chill rolls. The film is then grasped by grippers or edge grip rollers and transferred into an oven where it is oriented in transverse direction [38].

In this paper, structural development during film extension of PLA is studied, with emphasis on the comparison between simultaneous and sequential biaxial stretching.

2. Experimental

2.1. Material

Linear PLLA with number and weight molecular weights around 76,200 and 163,000 respectively, kindly provided by Dow–Cargill LLC, now Natureworks, was used for this research. 8% D component is randomly distributed in the chains to depress its melting point. As a result, T_m of this material ranges between 145 °C and 150 °C. T_g of PLA is around 60 °C. During heating from fully amorphous state, this material crystallizes at a temperature called cold crystallization temperature (T_{cc}) around 110 °C (experimental conditions are given in next section). Predried pellets of PLA were cast using Prodex single screw extruder equipped with an 8″ wide film die on to a casting roll cooled by water. DSC scan confirms that the crystallinity of as-cast film is negligible, as shown in Fig. 1. As shown in this figure, due to very slow crystallizability, PLA needs to be heated at slower rates to cold crystallize during the DSC scans. Both in-plane and out-of-plane retardations are found to be zero in as-cast films.

2.2. Thermal analysis

Thermal properties of the samples were measured with a Dupont 2920 differential scanning calorimeter in 0–180 °C range with 20 °C/min heating rate under dry nitrogen blanket. The samples were crimped into Aluminum pans to a total weight of 6–10 mg.

Crystallinity of the samples can be calculated with the equation below:

$$\text{Crystallinity}\ (\%) = \frac{\Delta H_{exp}}{\Delta H_f} \times 100\% \quad (1)$$

where $\Delta H_{exp} = \Delta H_{melting} - \Delta H_{cold\ crystallization}$, and ΔH_f is the heat fusion of 100% crystalline PLA, which was taken as 93 J/g [5]. The

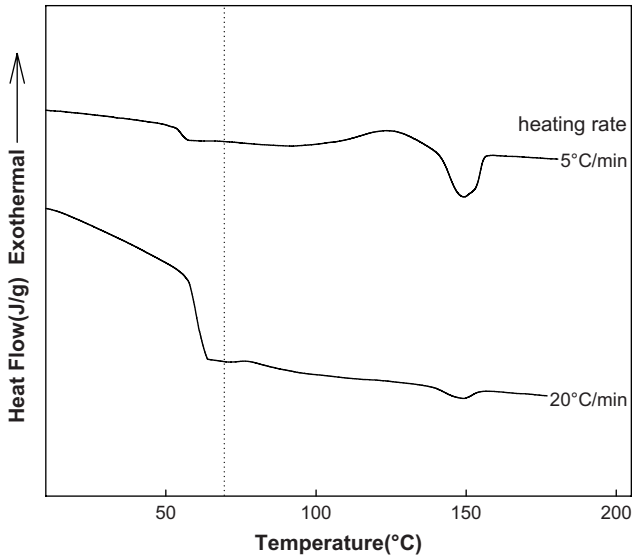

Fig. 1. DSC curves of as-cast films.

$\Delta H_{cold\ crystallization}$ peak represents the portion of the heat fusion induced by cold crystallization during DSC scan. This portion must be subtracted from the melting peak in order to obtain the original crystallinity of the sample before DSC scan.

2.3. Film stretching

An Iwamoto702 biaxial stretcher was employed in this research. The samples were gripped by 40 pneumatic clips and the gage separation distance between the clamps is chosen to be 12 cm × 12 cm. Film extension is carried out at 70 °C, which is about 10 °C higher than the glass transition temperature of the as-cast film. The cast films were first kept in the preheated chamber for 10 min for temperature equilibrium. Stretching rate was chosen to be 0.025 s^{-1}, which corresponds to 3 mm/s.

Three stretching modes were employed in this study, as shown in Fig. 2.

(1) Uniaxial constant width (UCW) stretching
(2) Simultaneous Biaxial (SB) Stretching
(3) Sequential Biaxial (SEQ) Stretching

In UCW mode, the films were stretched in MD while it is constrained in TD. In SB stretching, the films were simultaneously

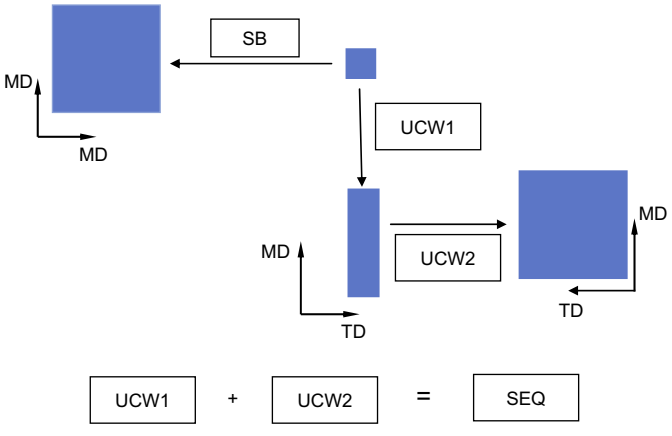

Fig. 2. Stretching modes employed.

stretched in two perpendicular directions at the same rate and to the same ratio. During SEQ stretching, the films are first stretched in MD in UCW mode, then, it is stretched in the perpendicular TD in UCW mode. Same stretching rate was used in MD and TD.

2.4. Stress vs. strain behavior

The apparent true stresses in both stretching directions are obtained by dividing the time variation of load observed by instantaneous cross-section area obtained from movement of the clamps assuming affine deformation and incompressibility of the samples.

2.5. Birefringence

In-plane and out-of-plane birefringences of the samples were measured with an optical bench equipped with a Gaertner Polaroscope and a Babinet compensator. This optical bench contains a goniometer, which enables the sample to be rotated. Out-of-plane birefringence is calculated using Stein's equations [39]:

$$\Delta n_{12} = -\frac{\lambda_0 R_0}{d_0} \tag{2}$$

$$\Delta n_{13} = -\frac{\lambda_0}{d_0}\left[\frac{R_0 - R_\varphi(1-\sin^2\varphi/\overline{n}^2)}{\sin^2\varphi/\overline{n}^2}\right] \tag{3}$$

$$\overline{n} = \frac{n_1+n_2+n_3}{3} \tag{4}$$

$$\Delta n_{23} = \Delta n_{13} - \Delta n_{12} \tag{5}$$

where λ_0 is the wavelength of the incident light, d_0 is the sample thickness. φ is the tilting angle. R_0 is the retardation obtained when incoming beam is vertical to the film plane. R_φ is the retardation of film tilted by angle φ. $\overline{n}$ represents the average refractive index of PLA, which is taken as 1.47 [19]. 1–3 represents MD, TD and ND respectively.

2.6. Wide angle X-ray diffraction (WAXD)

A Rigaku diffractometer was employed to illustrate the development of chain conformation in crystalline phase. The voltage and current were set to be 150 kV and 40 mA. A $\theta/2\theta$ scan in transmission mode from 27° to 34° 2θ was used to locate the peak position of (0 0 10) planes, which indicates the helical conformation of PLA chains in crystalline phase. During scanning, MD of the samples was oriented horizontally in the sample holder, allowing meridional scanning. Step size of the scan was chosen to be 0.02 and integration time was chosen to be 10 s.

Two-dimensional WAXD images were obtained in flat plate geometry using a Rigaku X-ray imaging system equipped with an 18 kW rotating anode X-ray generator with a Rigaku Imaging Plate. The films were stacked to a thickness of 1–1.5 mm. In order to assess the orientation behavior in biaxially extended films, two patterns were obtained with the X-ray beam directed in ND and MD with exposure of 15 min. Sample-to-detector distance was chosen to be 150 mm.

Pole figure of selected samples was obtained with a GE XRD-6 X-ray generator equipped with an automated quarter circle goniometer. Voltage and current of the X-ray tube on this GE X-ray unit were set to 30 kV and 30 mA respectively. For each combination of χ (chi) 5° and φ (phi) 10° step, 10 s integration time was used. The films were stacked to form 4 mm × 1.5 mm × 1.5 mm prism and were mounted on the goniometer with spindle axis parallel with MD. The combined crystalline diffractions of the (200) and (110) planes in crystalline phase were measured.

3. Results and discussion

3.1. Birefringence development

Because of its chiral nature, PLA is expected to have optical activity [40,41]. This activity is maximum when the light is propagated along the chain axis and relatively negligible normal to the chain axis (1000:1 ratio) [42,43]. In our measurements, the polymer chains are primarily oriented in the plane of the films and the measurements were performed with the light beams directed normal or near normal (~30°) to the film surfaces, therefore we neglected the effect of optical activity in birefringence measurements in this research.

Fig. 3 shows the in-plane (Δn_{12}) and two out-of-plane birefringences (Δn_{23} & Δn_{13}) of the simultaneous biaxially stretched films. In-plane birefringence remains zero throughout this mode of stretching indicating in-plane isotropy is preserved. And the film exhibits optically uniaxial symmetry as the two out-of-plane birefringences renaub equal and increase monotonously with deformation. These data indicate that the optic axis of these films remains normal to the film surface.

The UCW mode (Fig. 4) of stretching causes the materials to exhibit optically biaxial character as the Δn_{12} and Δn_{13} (1 = MD, 2 = TD, 3 = ND) exhibit systematic increase with λ_{MD} stretching, while exhibiting minor difference for each condition. The fact that we observed was very low but non-zero Δn_{23} in between the two directions attests to the presence of optical biaxial symmetry. Transverse stretching from two MD stretched states of 3 × 1 and 4 × 1 shown in Fig. 5 indicates that in-plane isotropy ($\Delta n_{12} = 0$) is attained at smaller deformation in the second stretching direction ($\lambda_{MD} > \lambda_{TD}$) unlike the simultaneous stretching mode indicated earlier. When stretched balanced biaxially in SEQ mode ($\lambda_{MD} = \lambda_{TD}$), the in-plane birefringence invariably becomes negative favoring the anisotropy in the second stretching direction. This is attributable to the fact that stress induced crystallites formed in the first stretching stage serve as physical cross-linking points, making

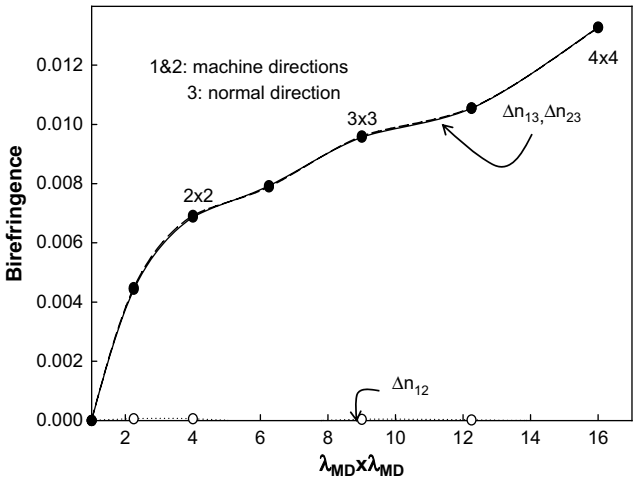

Fig. 3. Birefringence vs. $\lambda_{MD} \times \lambda_{MD}$ curve for Simultaneous Biaxially stretched (SB) films.

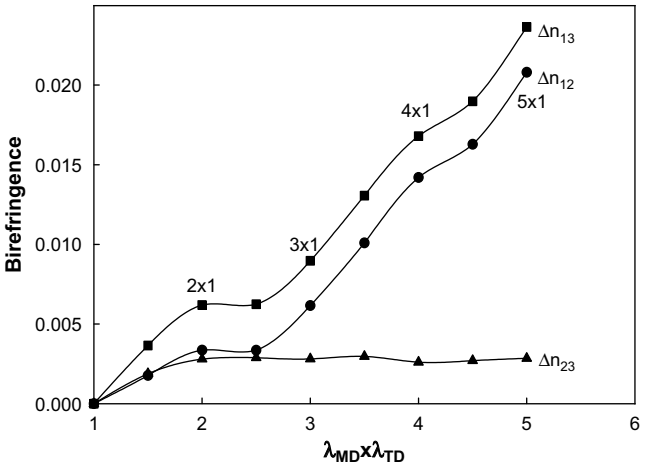

Fig. 4. Birefringence vs. $\lambda_{MD} \times \lambda_{TD}$ of UCW Samples ($\lambda_{TD} = 1$).

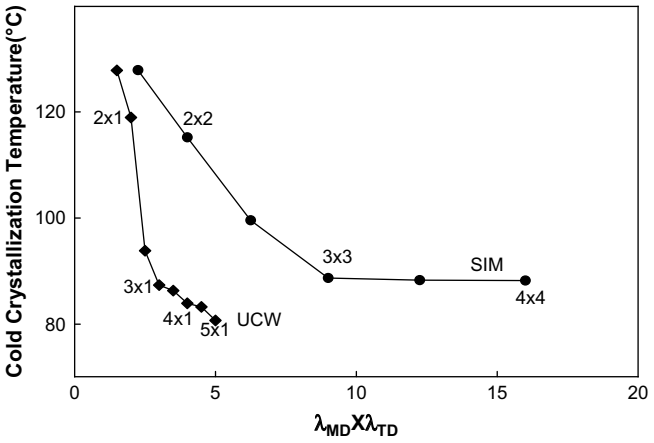

Fig. 6. Cold crystallization vs. λ_{MD} of UCW and SB samples.

transverse stretching more efficient as it will be discussed in detail below [27–29,44]. Out-of-plane birefringence (Δn_{23} 2 = TD, 3 = ND) monotonously increases with λ_{TD} (Fig. 5) as a result of the chain alignment in the film plane during the increase of λ_{TD}. Similar behaviors were observed in other polymers [11–18,20–22,45–52].

Intrinsic birefringence of amorphous PLA is reported to be positive around 0.03 [1–3], while intrinsic birefringence of crystalline PLA is controversial. The method based on the vectorial summation of bond polarizabilities for α crystals gives a value of −0.013, while experimental results indicate that a crystal possesses an intrinsic birefringence of 0.03–0.033 [19]. From Fig. 4, we can see that Δn_{13} approaches 0.025 at highest stretching ratio. Therefore, our result favors the experimental result of α crystal intrinsic birefringence to be positive (0.03–0.033), as discussed above.

3.2. Thermal analysis

During both UCW and SB stretching, crystallinity increases while cold crystallization temperature decreases with deformation, as shown in Figs. 6–9. In both UCW and SB stretched samples, heat flow of cold crystallization (area under this peak) first increases and then decreases with λ_{MD}. At low deformation levels, the increase of area under the cold crystallization is unusual for slow crystallizing polymers and we attribute this to quite sluggish nature of PLA chains to crystallize even during heating from the cold state during DSC experiments. As mentioned earlier, this sluggishness is partly due to the presence of 8% D component. In order for them to even cold crystallize, they need to be oriented, otherwise the PLA superheats without showing any thermal crystallization. Obviously this is a rate dependent phenomenon and utilization of slower heating rates would readily cause cold crystallization as it would give more time for chains to self-diffuse to crystallization fronts to facilitate growth (Fig. 1). With the gradual depletion of amorphous phase as a result of stress induced crystallization, this area eventually begins to decrease at high stretch ratios. Similar behaviors have been observed in other slow crystallizing polymers [20,21,23–29].

In sequential stretching, the first stage being uniaxial in character progressively increases the crystallinity (Fig. 8). At the initial stage of extension in TD, crystallinity increases slightly with λ_{TD}, as shown in Fig. 9. This is due to the fact that the transverse stretching tends to relax the chain segments oriented in MD, (a behavior akin to opening of accordion) loosening the overall structure and facilitating the registration of the oriented but uncrystallized chains into the crystals oriented in MD. Further extension in TD is found to eventually destroy the crystals. Extension in TD tends to disrupt the chain orientation in MD by disorienting them, leading to higher cold crystallization temperature, as exhibited in Fig. 9. This behavior reverses as λ_{TD} approaches λ_{MD}, developing secondary population of chains that register with each other and thus begin to form crystals. T_{cc} starts to decrease at highest deformation levels and this coincides with

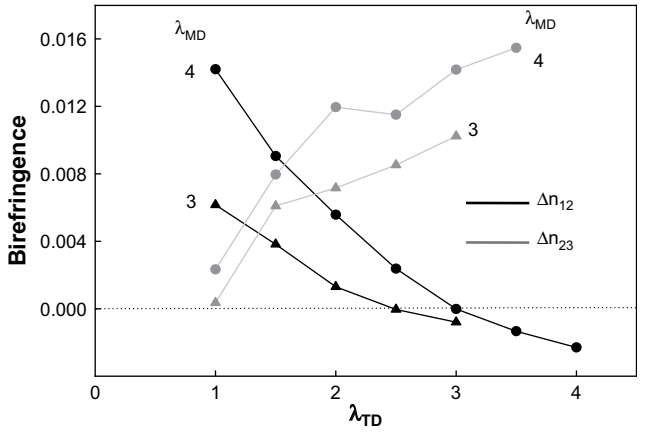

Fig. 5. Δn_{12} and Δn_{23} vs. λ_{TD} of Sequential biaxially stretched samples.

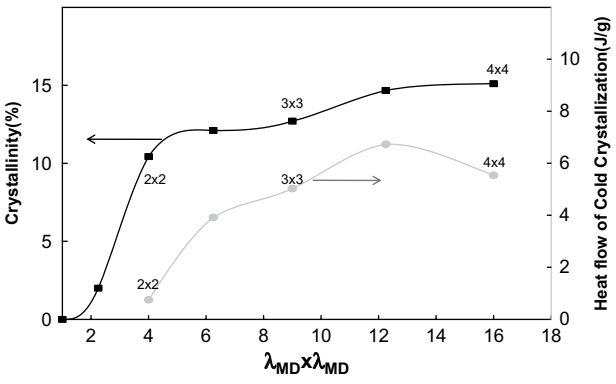

Fig. 7. Crystallinity and heat flow of cold crystallization vs. $\lambda_{MD} \times \lambda_{MD}$ curves of SB Samples.

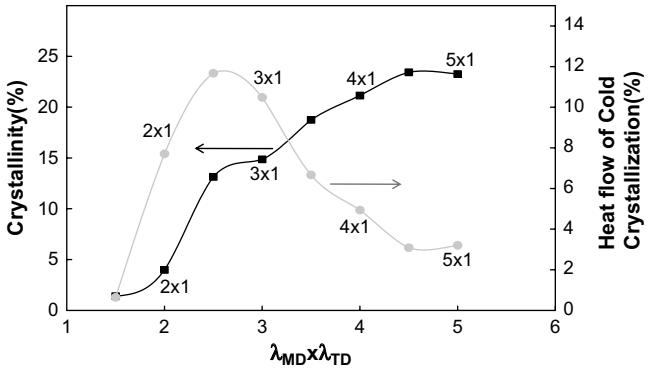

Fig. 8. Crystallinity and heat flow of cold crystallization vs. $\lambda_{MD} \times \lambda_{TD}$ curves of UCW Samples.

the increase in oriented second population and the crystallinity development in this second population. Others have reported similar behavior for PET [19,26–29].

3.3. Stress vs. strain behavior

In simultaneous biaxial stretching mode (SB) PLA exhibits a rubbery stress–strain behavior at 70 °C (Fig. 10). With deformation stress steadily increases ultimately leading to strain hardening. This strain hardening is critical for self-leveling of polymer films to ultimately obtain uniform thickness [34–38,45]. In UCW mode the stress increasingly becomes higher in MD while in the TD, this rise is delayed due to higher stretch ratios. (Fig. 11) Obviously the stress hardening occurs at lower λ_{MD} in SB mode than in the UCW mode. This is natural since area expansion rate is much higher during SB stretching.

The stress development in sequential biaxially stretched (SEQ) films is shown for two cases: One with first stretch ratio at 3×1 (Fig. 12) and the other with first stretch ratio at 4×1 (Fig. 13). The samples stretched to relatively lower stretch ratio in first direction (Fig. 12) show that the at the beginning of second stretching the stress in the first direction (MD) temporarily decreases at early stages of the second stretching while stress of the second direction (TD) shows a rapid rise. If the second stretching is applied on a sample with 4×1 first stretching, both stresses in MD and TD show a sharp rise though they cross each other at some intermediate deformation level. Transverse stretching is found to induce strain hardening even at the start of extension in TD. Similar behaviors have been reported in stress vs. strain behavior of PET [48–50].

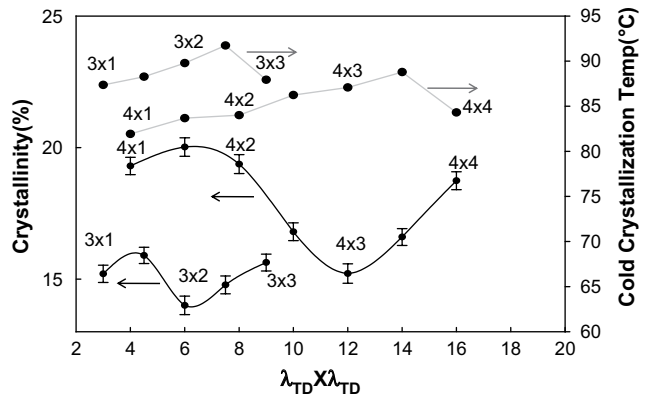

Fig. 9. Crystallinity and cold crystallization temperature vs. $\lambda_{MD} \times \lambda_{TD}$ for sequential biaxially stretched films.

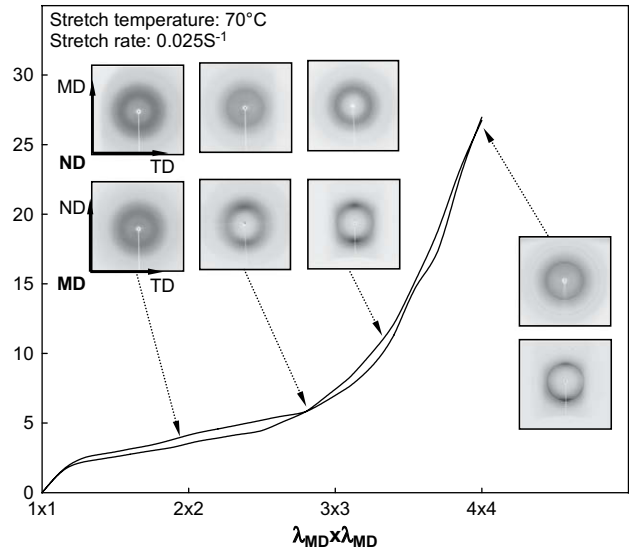

Fig. 10. Apparent true stress vs. $\lambda_{MD} \times \lambda_{MD}$ curve of SB sample.

3.4. WAXD

Typical oriented crystalline peaks for PLA are identified in Fig. 14. The WAXS patterns obtained at strategically selected samples of representing varying deformation conditions are also shown in Figs. 10–13 for SB, UCW and SEQ samples respectively. During SB stretching, the amorphous chains gradually orient in the film plane and beyond the onset of strain hardening the WAXS patterns with the X-ray beam taken along MD exhibit two very sharp meridional peaks superposed over the amorphous halo. The azimuthal spread of this peak is very narrow and it becomes even sharper at 3.5×3.5 condition. This type of pattern in the absence of other higher order peaks represents nematic-like order in the material indicating that in this mode the three-dimensional crystalline order is not established even well into the strain hardening range. At 4×4, a beginning of three-dimensional order is observed (Fig. 10). The WAXS patterns shown in Fig. 10 (bottom row) indicate that the chains do become oriented in the plane of the film. These regions do not exhibit developed crystalline evidenced by the absence of substantial number of diffraction peaks. This behavior is due to random orientation of the chain segments in the

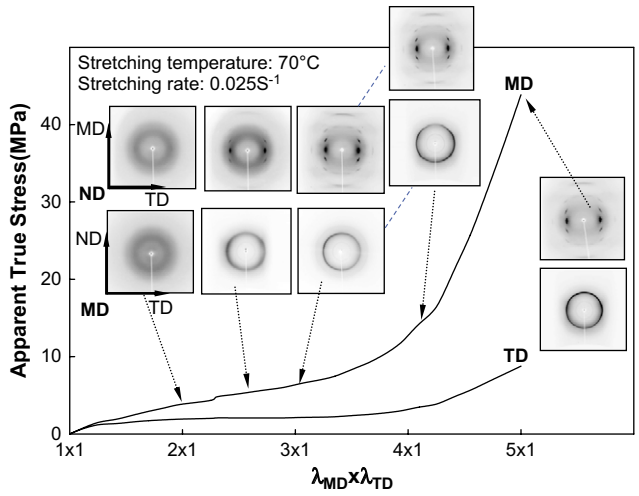

Fig. 11. Apparent true stress vs. λ_{MD} curve of UCW samples.

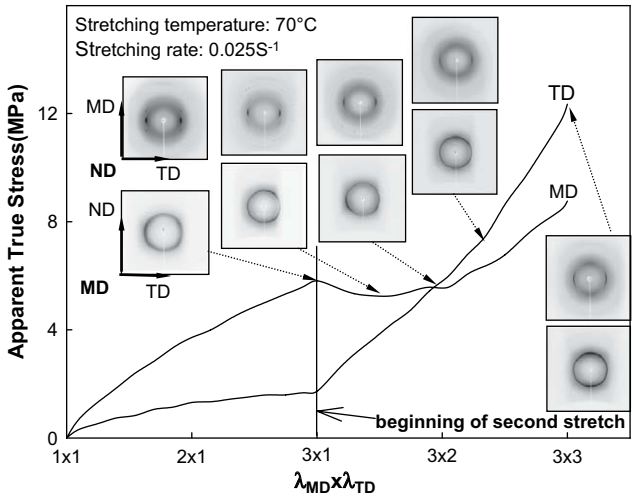

Fig. 12. Apparent true stress vs. $\lambda_{MD} \times \lambda_{TD}$ curve of SEQ samples with λ_{MD} of 3.

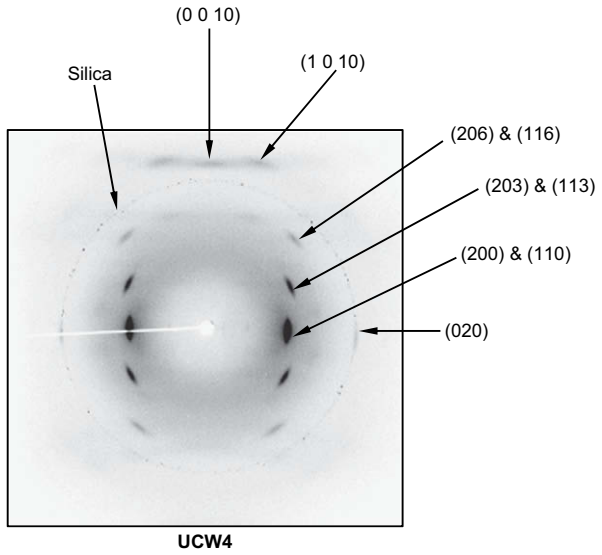

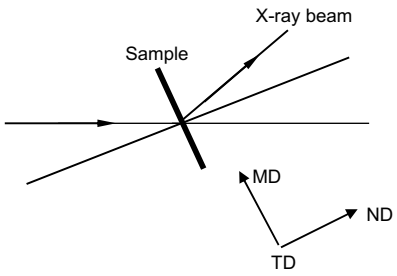

Fig. 14. Illustration of crystal planes.

film plane, thus they have less chance to become parallel with each other and crystallize. Obviously, this is aggravated by the absence of significant chain relaxation at the chosen processing temperature that is only 10 °C above the T_g. This behavior leads to low crystallinity and crystal perfection.

WAXS patterns through ND show uniform intensity (top row), in accord with birefringence data shown earlier signifying in-plane isotropy with the optic axis normal to the film plane [53–56]. The WAXS pole figure of the (200) (110) combination peak shown in Fig. 15 illustrates that the poles of these planes are primarily oriented in the ND. This is typical of SB stretching of many polymers [23–26,38,48–52,57,58].

During UCW stretching, a well-developed three-dimensionally ordered crystalline phase forms when λ_{MD} is between 2.5 and 3, (Fig. 11). Further stretching leads to very highly oriented and ordered crystalline structure. Analysis of the (0010) peaks through diffractometry (data not shown) indicates that the chains in the crystalline regions form helical conformation between 10/3 helix of α and 3/1 helix of β phase [6–10].

SEQ samples with very low λ_{TD} showed crystal orientation essentially similar to UCW samples, as shown in Figs. 12 and 13.

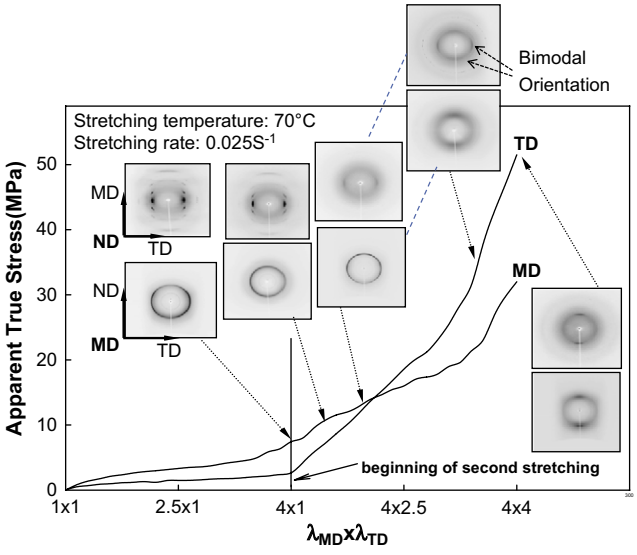

Fig. 13. Apparent true stress vs. $\lambda_{MD} \times \lambda_{TD}$ of SEQ samples with first stretch ratio of 4.

Further transverse stretching is found to decrease the orientation of the crystal population #1 in MD direction presumably as a result of increased splaying action under the transverse stretching, while creating totally new population oriented in TD with much poorer crystalline order, inducing a bimodal orientation. This is evidenced by the appearance of concentration of diffraction intensities both in meridian and equator in the WAXD pattern obtained with X-ray beam directed along the ND. In fact, this second population has such low order, it may be called oriented amorphous. Apparently, the crystals formed during UCW stretching served as physical cross-linking points during transverse stretching, preventing the segments from sliding along the entanglements. Therefore, we conclude that these films exhibit very unique in-plane bimodal "cross-hatched" orientation. Similar behaviors have been observed in PE and PEN [53–56]. As shown in Fig. 13, a well-developed highly

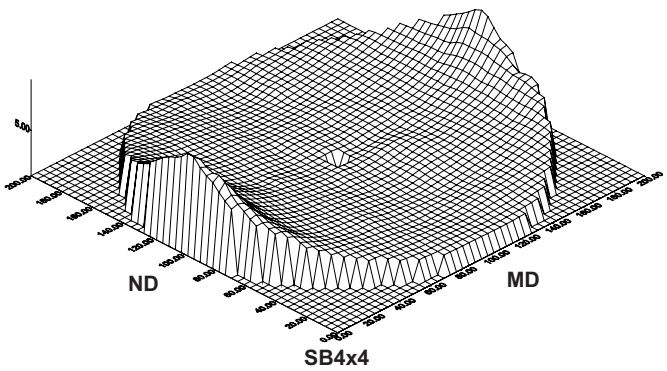

Fig. 15. Wide angle X-ray pole figure of SB sample.

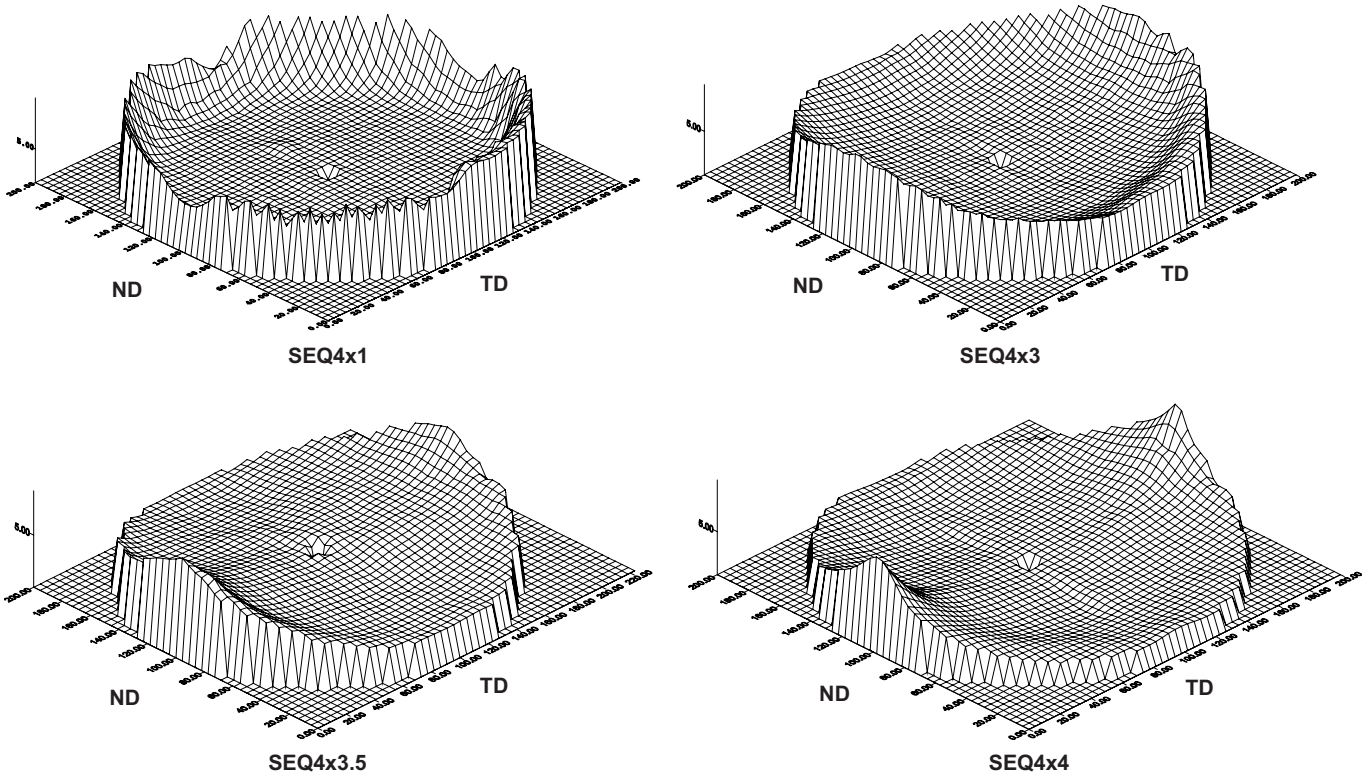

Fig. 16. Pole figure of SEQ samples.

oriented crystalline network is formed at λ_{MD} of 4 during the first stretching stage. This obviously forms a tightly knit long range connected network. This makes the stretching in the transverse direction quite efficient. As a result, the original crystalline regions formed along the MD are destroyed upon stretching in the transverse direction. At intermediate TD (e.g. 4×3) stretching ratios, this texture exhibits bimodal orientation with one population still oriented in the MD and second gradually forms in the Transverse direction. When 4×4 condition is reached, the population #1 oriented in MD essentially disappears, giving way to the population #2 primarily oriented in TD.

The WAXS pole figure of combination equatorial plane (200/110) of SB 4×4 stretched films is shown in Fig. 15 indicates that the chains exhibit perfect in-plane isotropy as the poles of these planes are all concentrated in the ND direction. In the case of sequential biaxially stretched films (Fig. 16) the in-plane isotropy appears to be obtained in unbalanced biaxial state (4×3.5) and at 4×4 condition the orientation is slightly more towards the TD as was also evident in the birefringence data discussed earlier.

The destruction of crystallites with transverse stretching is quantitatively reflected in the crystallite size measurements presented in Figs. 17 and 18 for (200)/(110) combination planes. For this analysis, WAXS line profiles were obtained in MD as well as in TD to assess the state of the crystallite sizes in these two specific directions. After the peak separation, Scherrer equation was used to calculate crystal sizes

$$L = \frac{K \cdot \lambda}{\beta_{1/2} \cos(\theta)}$$

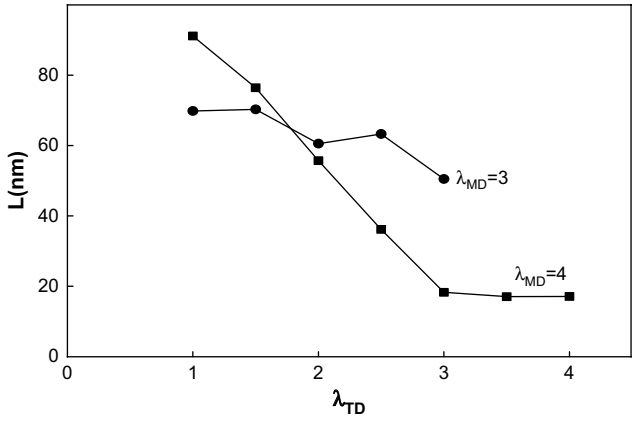

Fig. 17. Crystal size along [100] and [110] of crystals oriented along MD vs. λ_{TD} of SEQ samples.

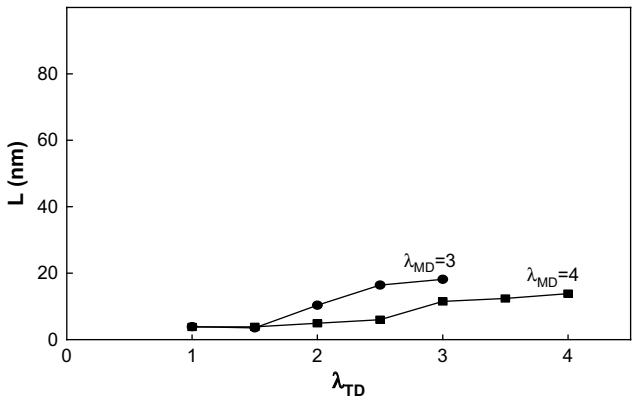

Fig. 18. Crystal size along [100] and [110] of crystals oriented along TD vs. λ_{TD} of SEQ samples.

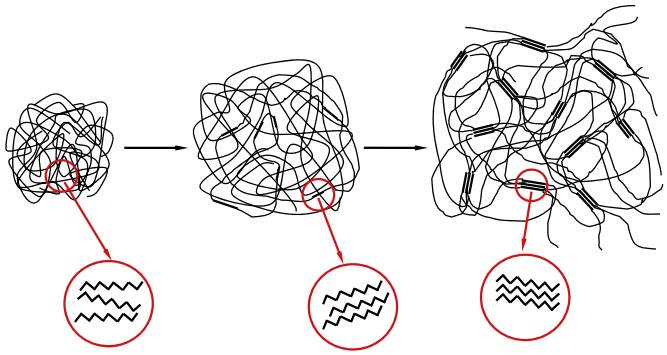

Fig. 19. Structural models for Simultaneous Biaxial (SB) stretching.

where $K = 1$, $\lambda =$ wavelength, $\beta =$ integral breadth in radians, $\theta =$ peak position.

While the crystallite size in the MD direction decreases dramatically at high λ_{TD}, [19,20,27–29] it slightly increases in the second population (Fig. 18). The crystalline order decreases faster in samples with $\lambda_{MD} = 4$ (Fig. 17). Clearly, this points to the fact that if the texture contains extensive crystalline phases leading to increased connected network, this helps in more efficient destruction upon transverse stretching rather than their rotation.

4. Structural interpretation

4.1. SB stretching

PLA chains are extended in film plane without preferred in-plane orientation during SB stretching, as shown in Fig. 19. SB stretching tends to orient the polymer chains in the plane of the film while maintaining in-plane isotropy. Efficiency of oriented crystallization is not very high as these in-plane randomly oriented chains have difficulty in finding chains of same orientation to crystallize. As a result, crystallites with very poor order are induced at intermediate stretch ratios. This crystallization improves as the deformation is increased. But we never observed fully developed three-dimensional order in the SB films.

4.2. UCW stretching

The chains become oriented along MD during UCW stretching, as indicated in Fig. 20. After certain level of orientation is reached, stress induced crystallization takes place, leading to the formation of a highly oriented crystalline phase. Upon further extension, further increase in fraction and perfection of crystalline phase was observed.

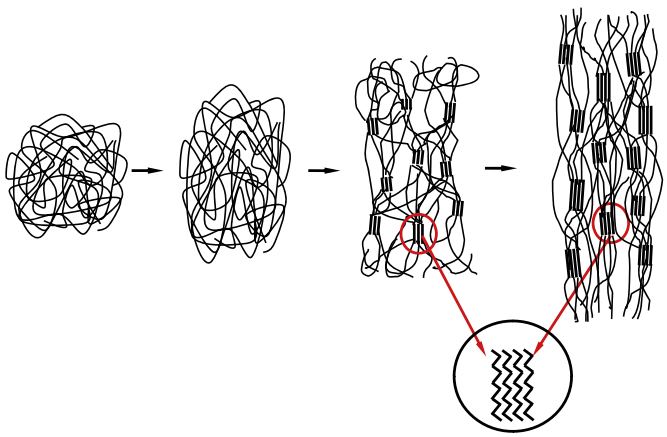

Fig. 20. Structural models for Uniaxial Constant Width (UCW) stretching.

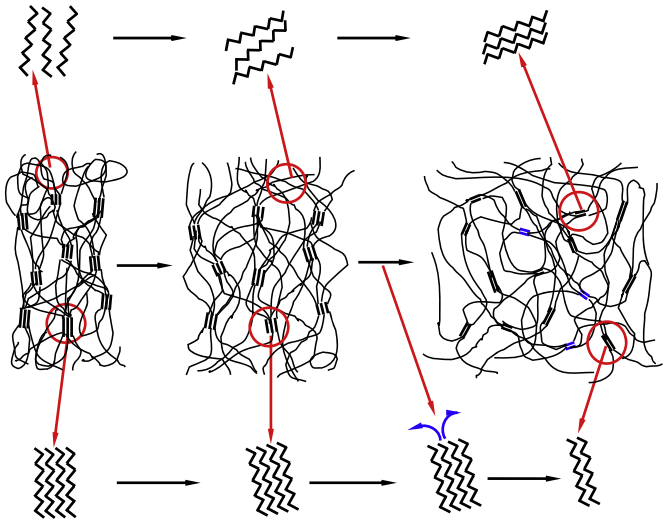

Fig. 21. Structural model of transverse stretching from $\lambda_{MD} = 3$.

4.3. Transverse stretching to UCW samples with a weak crystalline phase

When transverse stretching is applied to UCW samples at early stages of stress induced crystallization, the crystallite orientation decreases in MD as evidenced by the diffraction planes broaden in the azimuthal direction, while preserving the crystalline order. (Fig. 21). Higher levels of transverse stretching lead to partial destruction of crystallites originally oriented in MD the crystallites as they are pulled apart from each other, while another population with low structural order appears in TD. This texture has distinct bimodal texture with population #1 oriented in MD and population #2 oriented in TD. Much better structural order is observed in population #1, as compared to population #2.

4.4. Transverse stretching on UCW samples with a well-developed crystalline phase

When transverse stretching is applied to UCW samples with a well defined crystalline phase oriented in MD, similar structural development can be observed at initial stage of transverse stretching, as shown in Fig. 22. However, since the crystallites

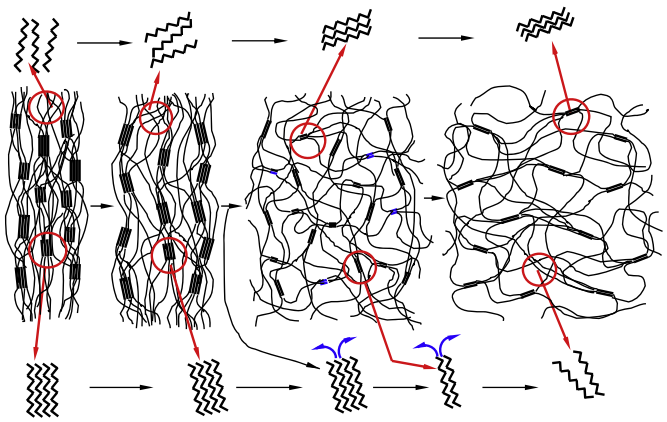

Fig. 22. Structural model of transverse stretching from $\lambda_{MD} = 4$.

formed during UCW extension along MD serve as physical cross-linking points, the transverse stretching becomes very efficient in transmitting lateral forces deep into the structure including all crystallites. Thus, the crystalline phase oriented in MD is destroyed at $\lambda_{TD} = \lambda_{MD}$, while the population oriented in TD forms poorly ordered crystalline phase.

5. Conclusions

Simultaneous biaxial stretching of PLA films in rubbery temperature ($T_g + 10\,^{\circ}C$) leads to in-plane isotropy with relatively poorly ordered crystalline regions. This is due to inefficient development of population of polymer chains of the same orientation adjacent to each other in this mode of deformation. This curtails the development of oriented crystallization (Fig. 19). At the processing temperature so close to T_g, the chain diffusion is too low to cause thermally induced crystallization. To produce commercially viable thermally stable SB films, they need to be further processed through dimensionally constrained heat treatment at a temperature where the thermal induced crystallization is fast.

Stretching in uniaxial constrained mode (UCW) leads to gradual development of orientation particularly beyond the strain hardening and consequent oriented crystallization with well-established three-dimensional order. The morphology development in the second stretching (TD) transverse to the first stretching depends on the state of the structure developed in the first stretching direction in UCW mode. If the crystallization is not well developed in the first stretching direction, the ease of reorientation of the crystalline regions towards TD is observed with minor damage to their integrity as the transverse direction stretching is applied. However, if the first stretching leads to substantial orientation and crystallinity, this structure, stretching in the transverse direction in the sequential biaxial mode leads to rapid destruction of these crystalline regions as the chains making up the crystalline regions are unraveled from the crystalline domains by the lateral forces quite efficiently. This leads to near complete disappearance of crystalline order at intermediate TD stretch ratios. If sufficient population of chains is oriented in the TD the crystalline order is reestablished. However, the order in these regions is generally poor requiring further constrained annealing to produce thermally stable oriented films.

References

[1] Datta Rathin, Tsai Shih-Perng. FEMS Microbiol Rev 1995;16:221.
[2] Lunt J. Polym Degrad Stab 1998;59:142.
[3] Garlotta D. J Polym Environ 2002;9:63.
[4] Amass AJ, N'Goala KLR, Tighe BJ, Schue F. Polymer 1999;40:5073.
[5] Fischer EW, Sterzel HJ, Kolloid ZZ. Polymere 1973;251:980.
[6] Hoogsteen W, Postenma AR. Macromolecules 1990;23:634.
[7] De Dantis P, Kovacs AJ. Biopolymers 1968;6:299.
[8] Kalb B, Pennings AJ. Polymer 1980;21:67.
[9] Kobayashi J, Asahi T. J Appl Phys 1995;77:2957.
[10] Cartier L, Lotz B. Polymer 2000;41:8909.
[11] Radhakrishnan J, Kaito A. Polymer 2001;42:3859.
[12] Kawai T, Muta M. Polymer 1992;33:2567.
[13] Jukherjee S, Jabarin Saleh A. Polym Eng Sci 1999;39:2419.
[14] Salem DR. Polymer 1998;39:7067.
[15] Buckley CP. J Appl Polym Sci 1990;41:1707.
[16] Boyce MC, Socrate S, Llana PG. Polymer 2000;41:2183.
[17] Arruda EM, Boyce Mary C. J Mech Phys Solids 1993;41:389.
[18] Hasan OA, Boyce MC. Polym Eng Sci 1995;35:331.
[19] Ohkoshi Y, Hirohiko Shira. Sen'i Gakkaishi 1999;55:62.
[20] Salem DR. Polymer 1992;33:3190.
[21] Doufas AK, Mchugh Anthony J, Miller Chester. J Non-Newtonian Fluid Mech 2000;92:27.
[22] Llana PG, Boyce MC. Polymer 1999;40:6729.
[23] Yeh GSY, Geil PH. J Macromol Sci Polym Phys Ed 1967;B1:251.
[24] Junugi T, Suzuki Akihiro, Hashimoto Minoru. J Appl Polym Sci 1981;26:1951.
[25] Lu XF, Hay JN. Polymer 2001;42:8055.
[26] Koening JL, Cornell SW. J Macromol Sci Polym Phys Ed 1967;1:279.
[27] Cakmak M, White James L. Polym Eng Sci 1989;29:1534.
[28] Cakmak M, Spruiell JE, White JL. J Polym Eng 1986;6:291.
[29] Cakmak M, Spruiell JE, White JL. Polym Eng Sci 1987;27:893.
[30] Flory PJ. J Chem Phys 1947;15:397.
[31] Fox TG, Flory Paul J, Marshall RE. J Chem Phys 1949;17:704.
[32] Fox TG, Flory Paul J, Marshall RE. Rubber Chem Technol 1950;23:576.
[33] Mchugh AJ. Polym Eng Sci 1982;22:15.
[34] Mina Hakkaraainen, Karlsson Sigbrit, Albertsson Ann-Christine. J Appl Polym Sci 2000;76:228.
[35] Studt E. German Patent 655,013; 1938.
[36] Reichel FH, Craven AE. US Patent 2,176,925; 1939.
[37] Kanai T, Gregory A. Campbell. Film processing. Hanser/Gardener Publications Inc.
[38] Alles FP, Heilman KA. U.S. Patent 2,728,941.
[39] Stein RS. In: Ke B, editor. Newer methods of polymer charaterization. New York: Intersecience Publishers; 1964.
[40] Kobay Yashi Jinzo, Massaki Ichiki. Ferroelectrics 1994;151:75.
[41] Kobayashi J, Asahi T. Ferroelectrics 1995;171:69.
[42] Kobayashi J, Fukada E. J Appl Phys 1995;77:2957.
[43] Tajitsu Y, Hosoya R. J Mater Sci Lett 1999;18:1785.
[44] Heffelfinger CJ, Burton RL. J Polym Sci 1960;47:289.
[45] Kokturk G, Cakmak M. Polym Eng Sci 2002;42:1619.
[46] Rietsch F. Eur Polym J 1990;26:1077.
[47] Chang H, Schultz JM. J Macromol Sci 1993;B32:99.
[48] Jabarin SA. Polym Eng Sci 1991;131:1071.
[49] Salem DR. Polymer 1995;36:3605.
[50] Salem DR. Polym Eng Sci 1999;39:2419.
[51] Simith F, Steward RD. Polymer 1974;15:283.
[52] Gohil RM, Salem DR. J Appl Polym Sci 1993;47:1989.
[53] Adams GC. J Polym Sci A-2 1971;9:1235.
[54] Cakmak M, Lee SW. Polymer 1995;36:4039.
[55] Cakmak M, Kim JC. J Appl Polym Sci 1997;65:2059.
[56] Bicakci S, Cakmak M. Polymer 1998;39:5405.
[57] Saburo Okajima, Kurihara Kazuhiko, Homma Keisuke. J Appl Polym Sci 1967; 11:1703.
[58] Hirozo Uejo, Sadao Hoshino J. Appl Polym Sci 1970;14:317.